A Synthetic Matrix with Independently Tunable Biochemistry and Mechanical Properties to Study Epithelial Morphogenesis and EMT in a Lung Adenocarcinoma Model

Bartley J. Gill[1], Don L. Gibbons[2,3], Laila C. Roudsari[1], Jennifer E. Saik[1], Zain H. Rizvi[2], Jonathon D. Roybal[2], Jonathan M. Kurie[2], and Jennifer L. West[1]

Abstract

Better understanding of the biophysical and biochemical cues of the tumor extracellular matrix environment that influence metastasis may have important implications for new cancer therapeutics. Initial exploration into this question has used naturally derived protein matrices that suffer from variability, poor control over matrix biochemistry, and inability to modify the matrix biochemistry and mechanics. Here, we report the use of a synthetic polymer-based scaffold composed primarily of poly(ethylene glycol), or PEG, modified with bioactive peptides to study murine models of lung adenocarcinoma. In this study, we focus on matrix-derived influences on epithelial morphogenesis of a metastatic cell line (344SQ) that harbors mutations in *Kras* and *p53* (*trp53*) and is prone to a microRNA-200 (miR-200)–dependent epithelial–mesenchymal transition (EMT) and metastasis. The modified PEG hydrogels feature biospecific cell adhesion and cell-mediated proteolytic degradation with independently adjustable matrix stiffness. 344SQ encapsulated in bioactive peptide-modified, matrix metalloproteinase–degradable PEG hydrogels formed lumenized epithelial spheres comparable to that seen with three-dimensional culture in Matrigel. Altering both matrix stiffness and the concentration of cell-adhesive ligand significantly influenced epithelial morphogenesis as manifest by differences in the extent of lumenization, in patterns of intrasphere apoptosis and proliferation, and in expression of epithelial polarity markers. Regardless of matrix composition, exposure to TGF-β induced a loss of epithelial morphologic features, shift in expression of EMT marker genes, and decrease in mir-200 levels consistent with EMT. Our findings help illuminate matrix-derived cues that influence epithelial morphogenesis and highlight the potential utility that this synthetic matrix-mimetic tool has for cancer biology. *Cancer Res; 72(22); 6013–23. ©2012 AACR.*

Introduction

Primary tumor invasion and metastasis is the leading cause of death in cancer patients, and epithelial–mesenchymal transition (EMT) is one principle mechanism driving metastasis. EMT is characterized by loss of epithelial polarity and intercellular adhesions and acquisition of mesenchymal features and migratory potential that permit invasion of tumor cells and dispersion to distant sites (1). The critical aspects of the tumor extracellular matrix (ECM) that promote or inhibit EMT and metastasis have not been fully characterized and remain an area of active investigation with potential for new therapeutic targets.

Initial exploration toward this goal has primarily focused on matrices from naturally derived materials such as collagen or Matrigel. It has been shown that increased density and organization of collagen-based matrices promote tumor progression *in vitro* and *in vivo* (2–4), and increased collagen cross-linking leads to EMT and invasion (5). Stiffening of Matrigel and collagen matrices perturbs epithelial morphogenesis of the MCF10A mammary cell line and promotes an invasive phenotype through alteration of integrin clustering and regulation of Rho activity and the FAK-ERK pathway (6; 7). Investigators have also begun to examine mechanical influences in synthetic matrix systems, but work thus far has largely been restricted to 2-dimensional (2D) culture on polyacrylamide gels (8–10).

A new lung adenocarcinoma model cell line panel has been developed in part to probe for similar ECM-related influences on lung cancer invasion and metastasis. These tumor cell lines, derived from a murine model with a somatically activated $KRas^{G12D}$ allele and a germline $p53^{R172H\Delta G}$ allele that produce primary lung adenocarcinoma with widespread metastatic disease (11), display an expression signature similar to that

Authors' Affiliations: [1]Department of Bioengineering, Rice University; and Departments of [2]Thoracic/Head and Neck Medical Oncology and [3]Molecular and Cellular Oncology, University of Texas M.D. Anderson Cancer Center, Houston, Texas

Note: Supplementary data for this article are available at Cancer Research Online (http://cancerres.aacrjournals.org/).

Corresponding Authors: Jennifer West, Department of Bioengineering, MS-142, Rice University, 6100 Main Street, Houston, TX 77005. Phone: 713-348-5955; Fax: 713-348-5877; E-mail: jwest@rice.edu; and Don L. Gibbons, Anderson Cancer Center, 1515 Holcombe Blvd., Unit 432, Houston, TX 77030, USA. Tel: 713-792-6363; Fax: 713-792-1220; E-mail: dlgibbon@mdanderson.org

doi: 10.1158/0008-5472.CAN-12-0895

of human tumors from non–small cell lung adenocarcinoma patients with poor prognosis (12). Metastatic cell lines from this model (e.g., 344SQ) transition from a mesenchymal to epithelial phenotype when encapsulated in Matrigel, forming highly polarized, lumenized spheres that undergo EMT upon TGF-β exposure because of repression of the microRNA (miR)-200 family (13). Repression of miR-200 is required for the cells to undergo EMT and metastasize in syngeneic animals and drives a coordinated set of proinvasive changes in the expression of cell surface proteins and ECM matrix proteins (14). In addition, *in vivo* interactions of the tumor cells with the surrounding microenvironment at the leading edge drives the Jagged2-dependent development of a metastatic subpopulation, clearly suggesting that lung cancer behavior and metastatic progression may be highly influenced by contextual cues from and interactions with the ECM (15).

While the ease of use and high bioactivity of naturally derived matrices such as Matrigel, collagen and fibrin have facilitated this work and that of the bulk of the field, these matrices suffer important disadvantages and limitations. Matrigel batch-to-batch variability makes comparisons between studies difficult, and even growth factor-reduced preparations suffer from a high degree of contamination from hundreds to thousands of growth factors presenting unknown and unknowable experimental confounders (16–18). Both Matrigel and collagen matrices exhibit weak mechanical strength ($E = 0.1–10$ kPa), limiting their relevance in the study of higher range elasticities that may be more typical of cancerous soft tissue ($E = 1–100$ kPa) or stiffer sites of common metastasis such as bone ($E >> 100$ kPa) and presenting handling difficulties with more involved experimental manipulations (19, 20). Further, they feature a critical flaw in that the adjustment of matrix mechanics almost always alters matrix biochemistry, presenting a significant confounder (20–23), particularly in studies that strive to parse out the relative importance of ECM ligand and stiffness influences.

Synthetic hydrogels composed of poly(ethylene glycol), or PEG, offer an alternative 3-dimensional (3D) culture environment that provides independent control over biophysical and biochemical cues. These materials are composed of bioinert polymer chains with defined chemical structure and end groups that enable cross-linking. In tissue engineering applications, they have been well characterized as biologically inspired ECM mimetics (18). PEG hydrogels are commonly formed through mild photoinitiated polymerization techniques that permit cell encapsulation with high viability, showing an advantage over other synthetic matrices such as polyacrylamide hydrogels, which incorporate a highly toxic monomer component that prevents translation to 3D (24).

Along with biocompatibility, PEG hydrogels offer easily tunable and well-controlled bioactivity. Given the high degree of hydrophilicity, neutrality, and mobility of PEG, these hydrogels are highly resistant to the protein adsorption that mediates cell attachment to most synthetic materials, allowing an unmodified hydrogel to act as a cell-noninteractive "blank slate" with any bioactivity only present through well-controlled experimental intervention. This tunability and their versatility in use with many different cell types have lead to their widespread use in tissue engineering applications (25–28). Importantly, because the system is modular and the mechanical component is distinct from the bioactive component, these matrices feature independently tunable mechanics and biochemistry with each factor available for testing of an independent biologic effect with high experimental control.

In this work, we used such a PEG-based hydrogel system to study lung adenocarcinoma cell lines from the $KRas^{G12D}/p53^{R172H\Delta G}$ murine model, with focus on a representative metastatic cell line, 344SQ, and compared its behavior in PEG matrices to that previously observed in the Matrigel system (13). We fabricated PEG hydrogels with varying elasticity and adhesive ligand concentration and probed for matrix-derived differences in epithelial morphogenesis and miR-200 regulation in response to TGF-β. In doing so we show that the more experimentally controllable synthetic hydrogel system is a useful tool for the cancer biologist to examine matrix-derived influences on tumor development and metastasis and an important improvement over the standard of the field.

Materials and Methods

Cell culture

The 344SQ, 393P, and 344P cell lines were derived from $KRas^{G12D}/p53^{R172H\Delta G}$ mice as previously described (11; 13). The 344SQ_429 cells are derived from 344SQ parental cells and contain a constitutive expression vector encoding the miR-200b_a_429 locus (13; 14). Cells and cell-laden hydrogels were cultured in a humidified atmosphere at 37°C and 5% CO_2 in RPMI 1640 (Mediatech) with 10% FBS (Atlanta Biologicals), 10 μg/mL gentamicin, and 0.25 μg/mL amphotericin B (Invitrogen).

Synthesis and purification of PEG-RGDS and PEG-PQ-PEG

Synthesis of PEG-RGDS has been previously described (26). Briefly, monoacrylate-poly(ethylene glycol)-succinimidyl carboxymethyl (PEG-SCM; Laysan Bio) and Arg-Gly-Asp-Ser peptide (RGDS; American Peptide) were mixed in dimethyl sulfoxide (Cambridge Isotope Laboratories) with a small volume of *N*, *N*-Diisopropylethylamine (DIPEA; Sigma) at molar ratios 1:1.2 and 1:2 (PEG-SCM: RGDS or DIPEA, respectively). After overnight reaction, the solution was dialyzed. PEG-PQ-PEG was synthesized by reaction with matrix metalloproteinase (MMP)-sensitive peptide GGGPQGIWGQGK (PQ). The PQ peptide was synthesized via standard Fmoc chemistry on an APEX 396 solid phase peptide synthesizer (Aapptec), characterized with MALDI-TOF, and then conjugated to PEG-SCM following a similar procedure as PEG-RGDS, but with a 2.1:1 molar ratio PEG-SCM:PQ. Conjugation of products was confirmed using gel permeation chromatography (Varian).

Cell encapsulation in hydrogels

Polymer mixtures were prepared sterilely with PEG-PQ-PEG ("PEG-PQ") and PEG-RGDS in 10 mmol/L HEPES buffered saline (pH 8.3) with 1.5% v/v triethanolamine (Fluka BioChemika), 3.5 μL/mL *N*-vinylpyrrolidone (Sigma) and 10 μmol/L eosin Y photoinitiator (Sigma). Unless otherwise noted,

PEG-PQ was mixed at 10% (w/v) and PEG-RGDS added at 3.5 mmol/L. 344SQ cells were pelleted by centrifugation at 500 × *g* for 4 minutes and then resuspended in the polymer solution at 1,500 cell/μL.

To create a hydrogel base for easy handling, cover glass was treated to introduce surface methacrylate groups as previously described (29). Hydrogel disks were fabricated by sandwiching a 5-μL droplet of polymer solution containing cells between a glass slide and a methacrylated glass cover slip separated by 380-μm-thick spacers and immediately exposing to white light for 30 s (Fiber-Lite Series 180, 150 W halogen, Dolan Jenner), leading to hydrogel polymerization and covalent linkage to the methacrylated cover glass base. High cell viability was confirmed 24 h after encapsulation (Live/Dead Kit, Invitrogen).

Mechanical testing

For material compressive properties, acellular hydrogel disks were formed as above using 5%, 10%, or 15% (w/v) PEG-PQ solutions. For comparison, Matrigel samples were prepared as previously described using a chamber plate with removable walls (13). Dimensions were obtained using digital calipers before subjecting samples ($n = 4$ per formulation) to compressive testing using an Instron Model 3340 mounted with a 10 N load cell. Instron Series IX/s software was used for testing control and data acquisition as uniaxial compressive strain was applied at 0.5 mm/min. Force-elongation data was converted to stress-strain data with corrected cross-sectional area and plotted to derive the elastic modulus from the slope of the linear portion of the curve.

344SQ sphere lumenization and size

344SQ cells were encapsulated in hydrogels with varied PEG-PQ concentration [5%, 10%, or 15% (w/v)] and fixed 3.5 mmol/L PEG-RGDS or with fixed 5% PEG-PQ concentration and varied PEG-RGDS concentration (1, 3.5, or 7 mmol/L) to assess matrix-related influences on the size and degree of lumenization of cell spheres. Hydrogel samples ($n = 5$ per formulation) were imaged every 2 days on an Axiovert 135 inverted fluorescent microscope (Zeiss), and sphere diameter was measured using Image J (NIH). Lumenization was quantified blinded to grouping as the number of spheres exhibiting central clearing over total spheres. Both size and lumenization data were expressed as means for all spheres in a given hydrogel sample. Further, size data from spheres across all hydrogel samples of a particular formulation were pooled and organized into histograms to better visualize matrix-related variation in sphere organization.

Immunohistochemistry

Hydrogel-encapsulated cells were fixed in 3.7% paraformaldehyde (EMS), permeabilized with 0.25% Triton X-100 (Sigma) and blocked overnight with 5% donkey serum (Sigma). Samples were then incubated with the following primary antibodies overnight at 4°C: mouse anti-β-catenin (BD Biosciences), mouse anti-α6-integrin (Chemicon), rabbit anti-ZO-1 (Invitrogen), rabbit anticleaved caspase-3 (Cell Signaling), or goat anti-ki-67 (Santa Cruz). Following rinse in PBS + 0.01% Tween (Sigma), samples were incubated overnight with an Alexafluor 488 or 555 tagged donkey anti-rabbit, mouse, or goat secondary antibody (Invitrogen), and counterstained with a 2 μmol/L 4′, 6-diamidino-2-phenylindole (DAPI) solution. Samples were imaged using a Zeiss 5Live confocal microscope.

Response to TGF-β and quantitative RT-PCR analysis

To observe responses to TGF-β, hydrogel-encapsulated 344SQ cells were cultured for 12 days to allow the formation of lumenized spheres, and then 5 ng/mL TGF-β1 (Calbiochem) was added to culture media. TGF-β-supplemented media was changed every 2 days. Samples were imaged on an Axiovert 135 inverted fluorescent microscope (Zeiss). Zymography was conducted to analyze for changes in MMP expression following TGF-β exposure using a 10% gelatin precast Ready Gel (BioRad) as previously described (25).

For RNA analysis, 344SQ cells were encapsulated at 3,000 cells/μL in hydrogels with matrix formulations as above ($n = 6$) and cultured for 10 days, after which half of the samples were treated for 4 days with TGF-β1 with daily supplemented media changes. Hydrogels were then digested with proteinase K (15 mg/mL, Calbiochem) for 2 minutes at room temperature, and then placed on ice before total RNA extraction with Trizol (Invitrogen) per manufacturer's protocol. Q-PCR was conducted on a 7500 Fast Real-Time PCR System (Applied Biosystems). The analysis of the miR-200 family levels (miR-200a, 200b, and 200c) and the mRNA for CDH1, CDH2, VIM, CRB3, and ZEB1 were conducted using TaqMan MiR assays (Applied Biosystems) and the data expressed relative to same-sample controls for miR-16 or L32, respectively.

Results

PEG hydrogel fabrication and biophysical characterization

Reaction of PEG-SCM with short, bioactive peptides–created pegylated peptides that were incorporated to render hydrogels bioactive (Fig. 1A). Cell adhesion was promoted through use of the fibronectin-derived RGDS peptide with incorporation of PEG-RGDS as a scaffold pendant group. To enable cell-mediated proteolytic degradation of the base hydrogel, the MMP-2 and -9–degradable PQ peptide (30; 31) was similarly reacted to create a PEG-PQ molecule wherein the peptide is flanked by 2 monoacrylated PEG chains. PEG-based hydrogels composed of polymer chains of similar size as PEG-PQ possess water content more than 90%, volumetric swelling ratios (Q) of 10 to 20, and cross-link densities (ρ_x) of 0.5 to 1.5 mol/L, with molecular weight between cross-links (M_c) and mesh size sufficiently large to permit free diffusion of most biomolecules (respectively, ∼1,000 g/mol and 50–100 Å; refs. 32; 33). The mechanics of the hydrogel network were determined to be dependent on the amount of incorporated PEG-PQ. A series of hydrogels with increasing PEG-PQ concentration was subjected to uniaxial compressive mechanical testing to determine the elastic moduli, a measure of material stiffness (Fig. 1B). Five percent, 10%, and 15% PEG-PQ matrices had compressive moduli of 21 ± 6, 42 ± 8, and 55 ± 11 kPa, respectively. To provide context with previous work, Matrigel samples were also tested and found to be much softer than these PEG formulations with a compressive modulus of approximately 2.5 kPa. Encapsulation of cells did not significantly change the

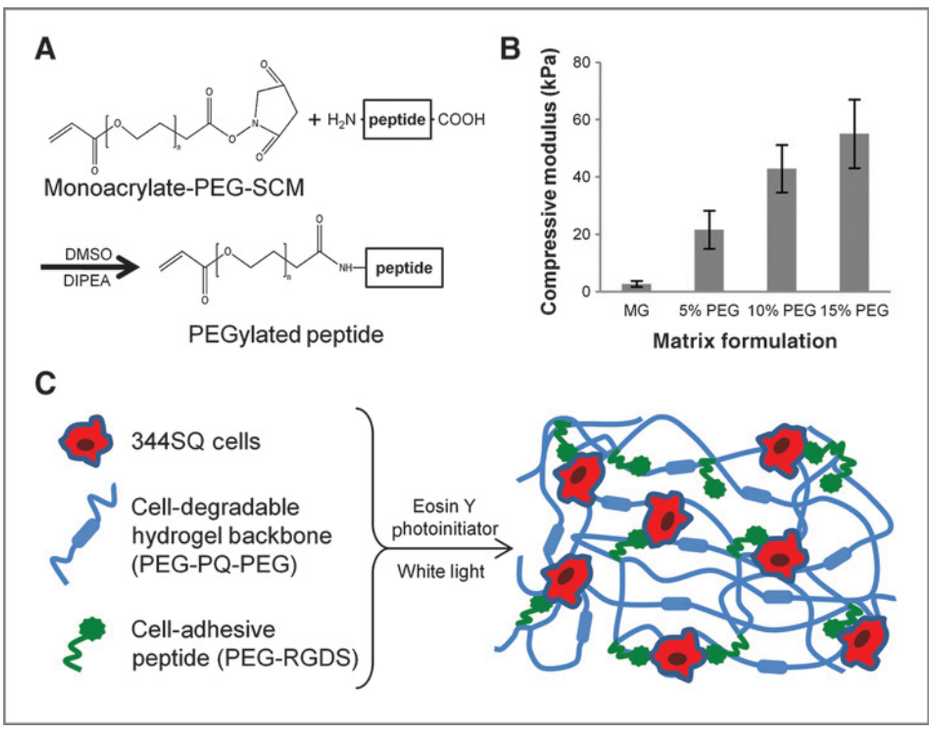

Figure 1. Bioactive PEG matrix with tunable mechanical properties. A, bioactive peptides are reacted with monoacrylate-PEG-SCM to form pegylated peptides: PEG-RGDS to permit cell adhesion and, with a 2-molar excess of PEG-SCM, PEG-PQ-PEG that serves as a matrix backbone susceptible to cell-mediated degradation via cleavage by MMP-2 and 9. B, elastic moduli derived from uniaxial compressive testing show matrix stiffness can be tuned by altering weight percent PEG incorporated in the polymer mixture. All PEG matrices are stiffer than Matrigel (MG; $P < 0.01$). C, matrix components are mixed with 344SQ cells and a photoinitiator and polymerized to form a PEG hydrogel featuring independently tunable matrix stiffness and adhesive ligand concentration with encapsulated cells interacting with bioactive components.

difference in elastic moduli between hydrogels of different PEG-PQ concentrations (Supplementary Fig. S1).

3D culture in bioactive PEG hydrogels recapitulates epithelial morphogenesis seen in Matrigel

Parental 344SQ lung adenocarcinoma cells were encapsulated in PEG-based hydrogel matrices by mixing with cell-degradable PEG-PQ and cell-adhesive PEG-RGDS in buffer in the presence of the photoinitiator eosin Y (Fig. 1C). The mild cross-linking conditions enabled high cell viability and, over several days in culture, cells proliferated, and formed multicellular spheres. After 7 to 10 days in culture, the cell clusters in PEG hydrogels (10% PEG-PQ/3.5 mmol/L PEG-RGDS) showed central clearing and formation of a

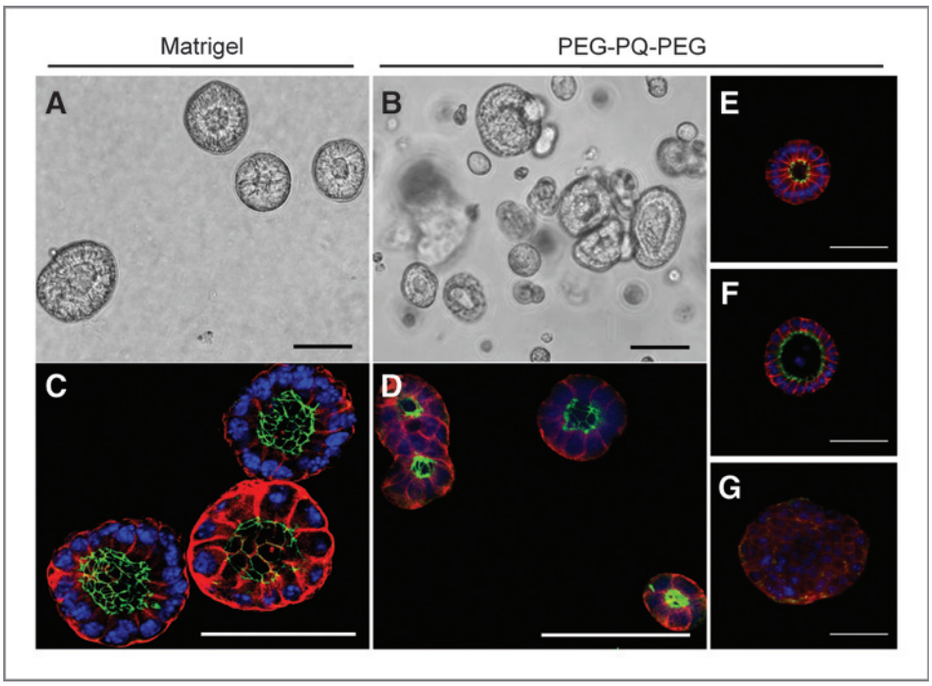

Figure 2. Culture in PEG matrix recapitulates 3D culture in Matrigel. A and B, bright-field images of 344SQ WT cells encapsulated in Matrigel (A) or a 10% PEG-PQ/3.5 mmol/L PEG-RGDS matrix (B) after 10 days in culture show sphere lumenization. C and D, staining for basolateral marker α6-integrin (red) and apical marker ZO-1 (green) in 344SQ cells encapsulated in Matrigel (C) and PEG (D) indicate that spheres have adopted organized epithelial polarity. E to G, staining for polarity markers β-catenin (red) and ZO-1 (green) of 344P (E), 429 (F), and 393P (G) cells encapsulated in PEG-PQ matrices recapitulate morphology and polarity seen in 3D Matrigel culture (13). DAPI, blue. Scale bar, 50 μm.

lumen surrounded by an organized layer of single cells reminiscent of the lung acinus, closely mirroring the morphology seen in Matrigel (Fig. 2A and B). Cells encapsulated in the PEG-based matrix formulation generally formed smaller spheres (~40 μm) than those in Matrigel (~80 μm) and took longer to lumenize (7–10 days vs. 6–8 days, not shown; refs. 13).

To assess the extent of epithelial morphogenesis, structures were stained for epithelial polarity markers: α6-integrin marking the basolateral surface and zonula occludens-1 (ZO-1) for apical tight junctions. Lumenized PEG-encapsulated spheres showed distinct separation of polarity markers demonstrating clear formation of basolateral-apical polarity in a staining pattern comparable to that seen for Matrigel-encapsulated structures (Fig. 2C and D) and suggesting a mesenchymal-to-epithelial transition (MET). To show the PEG system as a reliable 3D culture platform across cancer models, other adenocarcinoma lines previously studied in Matrigel were encapsulated and stained for epithelial polarity markers β-catenin (basolateral) and ZO-1 (Fig. 2E–G). Another metastatic cell line derived from a primary tumor of $KRas^{G12D}/p53^{R172H\Delta G}$ mice (344P) and the 344SQ_429 transfectant that constitutively expresses the miR200b_a_429 locus both formed lumenized spheres with epithelial polarity (Fig. 2E and F), whereas cells from the metastasis-incompetent 393P cell line formed disorganized cell aggregates (Fig. 2G), all of which mimics their respective behavior in Matrigel (13).

Matrix stiffness influences epithelial morphogenesis

Having established that a PEG-based system was capable of recapitulating the key epithelialization behavior exhibited by 344SQ in 3D Matrigel culture, we sought to examine the influence of key matrix parameters on this behavior. First, the PEG-PQ concentration, which forms the bulk of the material, was varied at 5%, 10%, or 15% while maintaining the cell-adhesive PEG-RGDS at a fixed 3.5 mmol/L. Utilizing higher polymer concentrations increased cross-link density and decreased mesh size, producing a stiffer matrix. Multicellular spheres formed in all matrix formulations, but spheres showed important differences in morphology and epithelialization behavior (Fig. 3A–C), with larger spheres and a lower percentage of lumenized structures in the softer, 5% PEG-PQ matrices. Monitoring sphere diameter with time (Fig. 3D) revealed that structures underwent rapid growth in the first few days of culture regardless of matrix stiffness, but growth persisted through day 8 only in the softer matrix (21 kPa), yielding spheres that were significantly larger relative to the other formulations (~80 μm in 21 kPa hydrogels vs. ~35 μm in the other formulations). An inverse relationship was observed for sphere lumenization (Fig. 3E); whereas all matrices exhibited

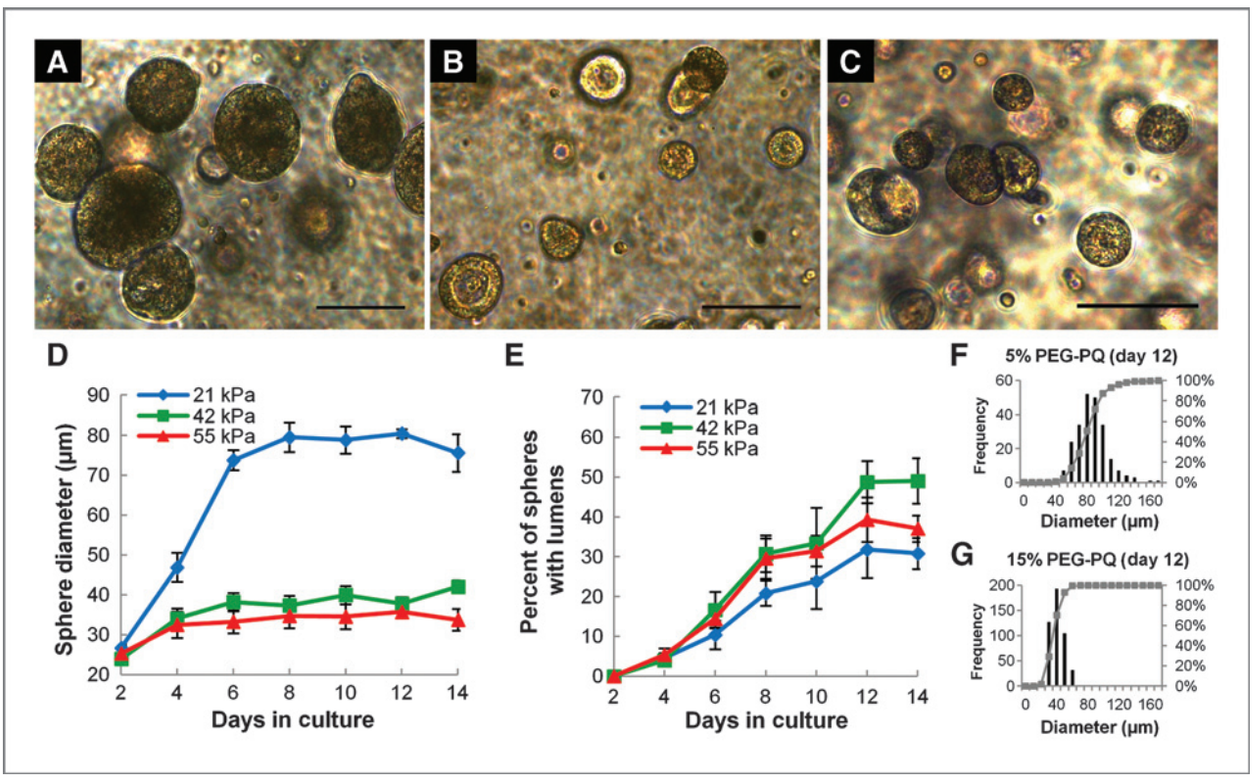

Figure 3. Matrix stiffness influences epithelial morphogenesis. A–C, bright-field images of spheres at 12 days in culture in 5% PEG-PQ (A; 21 kPa),10% PEG-PQ (B; 42 kPa), and 15% PEG-PQ (C; 55 kPa) matrices with 3.5 mmol/L PEG-RGDS show differences in sphere size and lumenization. D, significantly larger spheres form in the softer hydrogel (day 12, 21 kPa vs. others, $P < 0.01$), whereas in E, a higher degree of lumenization occurred in stiffer matrices (day 12, 42 kPa compared with 21 kPa, $P < 0.05$). F and G, histograms of pooled size data for all spheres in all samples show much greater heterogeneity in sphere development in softer hydrogels. Scale bar, 100 μm.

increasing lumenization throughout the culture period, fewer encapsulated spheres were lumenized in the 21 kPa matrix (35%) compared with the 42 kPa matrix (50%). It was also observed that spheres in the 21 kPa matrix tended to be more heterogeneous in size and morphology relative to the stiffer matrix formulations, as reflected in histograms of pooled size data showing greater variation in sphere diameter in the softer gel (Fig. 3F and G and Supplementary Fig. S2). Additional exploration of sphere size differences indicated that cells in spheres in 21 kPa matrices were slightly larger than those in 42 kPa matrices (cell area at maximum sphere cross-section, 87.5 $\pm$ 22.7 μm^2 vs. 63.6 $\pm$ 13.7 μm^2, not significant) and, more notably, the number of cells in 21 kPa matrix spheres was greater than that in 42 kPa matrix spheres (cell number at maximum sphere cross-section, 22 ± 4 vs. 8 ± 2, $P < 0.05$), both contributing to overall differences observed in sphere diameter. This size difference may also be reflective of a difference in epithelial organization; work in other systems suggests that a transition to larger, less uniform structures indicates loss of epithelialization (6).

Samples from spheres grown in the hydrogel matrices were stained for proliferation/apoptosis and polarity markers to more closely assess matrix stiffness-related influences in sphere development and epithelialization (Fig. 4). Ki-67 staining revealed diffuse proliferation throughout spheres encapsulated in soft matrices at day 4 (Fig. 4A), whereas spheres in stiffer matrices exhibited a more localized peripheral staining pattern (Fig. 4B). Proliferation persisted through day 6 in 21 kPa matrices (Fig. 4C), but decreased in stiffer matrices as spheres became more completely lumenized (Fig. 4D). These observations correlated with differences in apoptosis as spheres in softer matrices showed unlocalized caspase-3 activity (Fig. 4C), whereas spheres in stiffer matrices showed strong core caspase activity (Fig. 4D). Furthermore, at day 6 the epithelial markers β-catenin (basolateral) and ZO-1 (apical) remained disorganized in softer matrices (Fig. 4E), whereas spheres in stiffer matrices (Fig. 4F) showed peripheral nuclear alignment and polar organization, albeit incomplete as β-catenin persisted on the apical edge. By day 12, however, lumenized spheres were found in both soft (Fig. 4G) and stiff (Fig. 4H) matrices, with these spheres exhibiting a high degree of epithelial organization and clear segregation of polar markers.

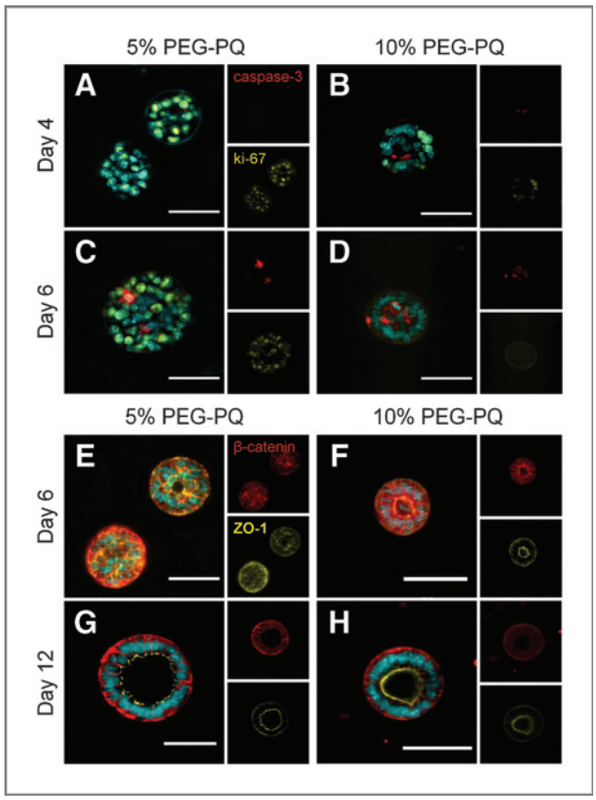

Figure 4. Matrix stiffness influences apoptosis and proliferation in developing spheres and degree of epithelial polarity. A–D, staining for cleaved caspsase-3 (red) and ki-67 (yellow) at day 4 (A and B) and day 6 (C and D) in 5% (A and C) and 10% (B and D) hydrogels show earlier localization of proliferation at sphere periphery (B) in the stiffer hydrogel and high core apoptosis activity to induce more rapid lumenization (D) compared with diffuse proliferation activity (A) and unlocalized apoptosis (C) in softer hydrogels. E–H, staining for polarity markers β-catenin (red) and ZO-1 (yellow) at day 6 (E and F) and day 12 (G and H) in 5% (E and G) and 10% (F and H) PEG-PQ hydrogels shows polar organization in spheres in only stiff hydrogels (F) at early time points compared with disorganization in softer hydrogels (E), whereas at later time points, lumenized spheres in both softer and stiffer matrices show a high degree of organized polarity (G and H) with a notable absence of basolateral β-catenin on the apical edge. DAPI, cyan. Scale bar, 50 μm.

Adhesive ligand concentration influences epithelial morphogenesis

We next evaluated cell adhesive ligand concentration in the absence of changes to matrix stiffness, encapsulating 344SQ in matrices with a fixed 5% PEG-PQ concentration (21 kPa) and PEG-RGDS at 1 mmol/L (Fig. 5A), 3.5 mmol/L (Fig. 5B), or 7 mmol/L (Fig. 5C). Although spheres initially grew rapidly in all matrices, average sphere diameters (Fig. 5D) in 7 mmol/L PEG-RGDS matrices increased to only around 60 μm through day 6, whereas spheres in matrices with lower concentrations of adhesive ligand grew more rapidly and persistently up to 80 to 90 μm in diameter. The percentages of spheres lumenizing (Fig. 5E) showed a strong relationship with adhesive ligand concentration; spheres rapidly and more completely lumenized in 7 mmol/L PEG-RGDS, whereas after 12 days in culture a very low percentage of spheres (15%) lumenized in the 1 mmol/L group. It was also observed that incorporation of high concentrations of adhesive ligand into matrices induced formation of a much more homogenous sphere population (Fig. 5F and G). Supporting our interpretation that these changes are ligand-dependent, incorporation of varying amounts of PEG-RGDS did not result in changes to hydrogel mechanical properties (1 mmol/L 18.5 $\pm$ 4.6 kPa vs. 7 mmol/L 19.2 $\pm$ 3.8 kPa, not significant).

To further assess the influence of adhesive ligand concentration on epithelial morphogenesis, spheres in 21 kPa matrices with either 1 or 7 mmol/L PEG-RGDS were stained for markers of proliferation, apoptosis, and epithelial polarity (Fig. 6). While proliferation was extensive at day 4 in matrices with low PEG-RGDS concentration (Fig. 6A), it exhibited no localization pattern, whereas matrices with high PEG-RGDS induced more

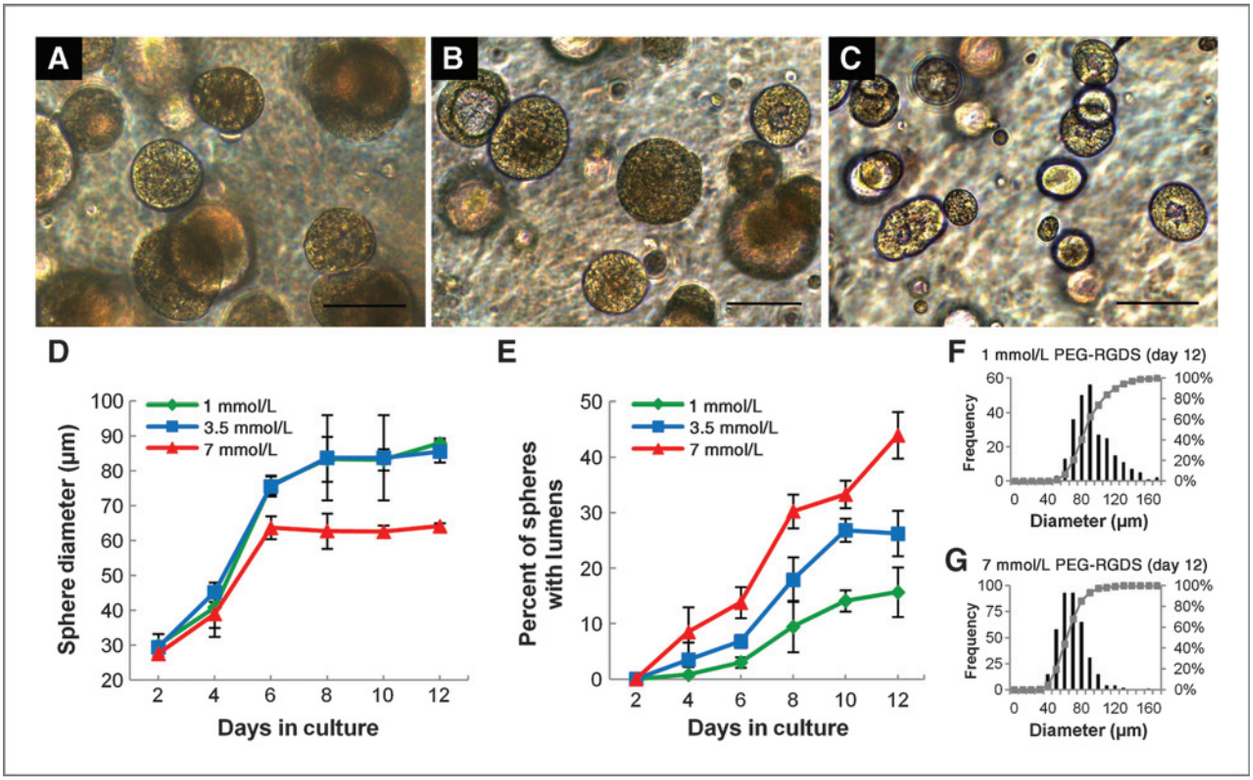

Figure 5. Adhesive ligand concentration influences epithelial morphogenesis. A–C, bright-field images of spheres at 12 days in culture in 5% PEG-PQ gels with PEG-RGDS at a concentration of 1 mmol/L (A), 3.5 mmol/L (B), or 7 mmol/L (C) show differences in sphere size and lumenization. D, smaller spheres formed in matrices with a high PEG-RGDS concentration (7 mmol/L vs. others, $P < 0.01$ at day 12), whereas in E, lumenization occurred more rapidly and completely in spheres encapsulated in matrices with higher PEG-RGDS concentrations (day 12, 7 mmol/L vs. others, $P < 0.01$ and 3.5 mmol/L vs. 1 mmol/L, $P < 0.05$). F and G, histograms of pooled size data show greater heterogeneity in sphere development in hydrogels with little adhesive ligand. Scale bar, 100 μm.

complete epithelial development with structures already exhibiting proliferation at the sphere periphery and central caspase-3 activity (Fig. 6B). At day 6, both sphere proliferation and apoptosis activity was scattered and diffuse in 1 mmol/L PEG-RGDS matrices (Fig. 6C). Meanwhile, structures in 7 mmol/L matrices had already developed into well-lumenized spheres (Fig. 6D). These observed differences in sphere development led to changes in epithelial organization; spheres in 1 mmol/L PEG-RGDS matrices adopted irregular morphologies by day 6 with spotty and unorganized expression of the basolateral and apical markers, β-catenin and ZO-1, respectively (Fig. 6E), whereas spheres in 7 mmol/L hydrogels formed lumens and developed appropriate apical-basal polarity (Fig. 6F). Well-organized spheres with clearly segregated polar edges were widely prevalent by 12 days in 7 mmol/L PEG-RGDS matrices (Fig. 6H). Although some spheres did lumenize in matrices with low concentrations of adhesive ligand, polarity markers remained disordered and morphology irregular with nuclei failing to arrange neatly around a cleared central lumen (Fig. 6G).

TGF-β induces EMT-related morphologic and epigenetic changes

Consistent with their metastatic behavior *in vivo*, TGF-β has been shown to initiate EMT in well-organized structures of 344SQ cultured in Matrigel through downregulation of miR-200 family member expression, inducing hyperproliferation, lumen filling, and matrix invasion (13). Probing for similar changes in spheres encapsulated in a PEG-based matrix (Fig. 7), lumenized spheres were allowed to form in matrices composed of 5% PEG-PQ with 7 mmol/L PEG-RGDS (Fig. 7A) and then exposed to soluble TGF-β. After 1 day of exposure (Fig. 7B), spheres began to lose organization and lumen clarity with epithelial organization continuing to diminish through 4 days of exposure (Fig. 7C) at which point lumens were completely filled. After 4 days of exposure, 0% of spheres were lumenized, polar organization was lost, and cells exhibited random proliferative and apoptotic activity (Supplementary Fig. S3). However, TGF-β response was not accompanied by a detectable increase in MMP expression (Supplementary Fig. S4).

To examine EMT-related microRNAs that may drive this morphologic change, quantitative RT-PCR was conducted to measure the changes in miR-200 levels and EMT markers following TGF-β treatment of spheres in matrices with fixed PEG-RGDS and varied PEG-PQ (Fig. 7D–G) or matrices with fixed PEG-PQ and varied PEG-RGDS (Fig. 7H–K). Regardless of matrix composition, miR200b levels were elevated before TGF-β and fell after exposure, coincident with the morphologic changes observed and similar to that seen in Matrigel-encapsulated spheres. Levels of miR-200a and miR-200c followed a similar pattern of decreased expression (Supplementary

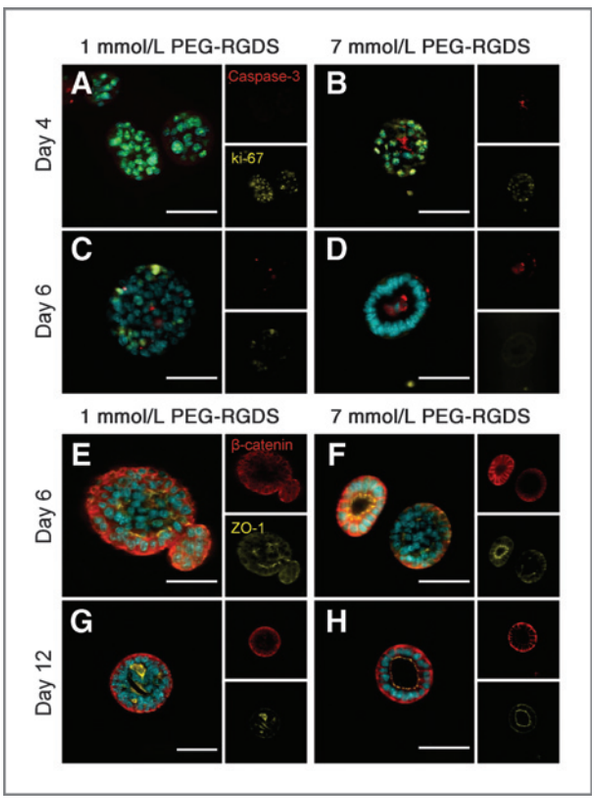

Figure 6. Adhesive ligand concentration influences apoptosis and proliferation in developing spheres and degree of epithelial polarity. A–D, representative images stained for cleaved caspsase-3 (red) and ki-67 (yellow) at day 4 (A and B) and day 6 (C and D) in 5% PEG-PQ hydrogels with 1 mmol/L (A and C) or 7 mmol/L (B and D) PEG-RGDS. Early peripheral proliferation and central apoptosis localization is evident with higher adhesive ligand concentrations (B) followed by rapid and organized lumenization (D), whereas spheres in matrices with low adhesive ligand concentration show a high degree of proliferation (A) and unlocalized apoptotic activity (C). E–H, representative images stained for polarity markers β-catenin (red) and ZO-1 (yellow) at day 6 (E and F) and day 12 (G and H) in 5% matrices with PEG-RGDS at 1 mmol/L (E and G) or 7 mmol/L (F and H) show the appearance of spheres with polar organization at early time points in matrices with high adhesive ligand concentration (F) with completely polar structures widespread at later time points (H). Spheres in hydrogels with low adhesive ligand concentration do not show organized polarity at early time points (E), and, at later time points, spheres that do display lumenization and polarity (G) have adopted less organized, more irregular morphologies. DAPI, cyan. Scale bar, 50 μm.

Fig. S5), indicating widespread epigenetic changes following TGF-β as miR-200b and miR-200c are found at 2 different chromosomal loci. Similarly, in all matrices, expression of epithelial marker genes decreased (*CDH1* and *CRB3*) as expression of mesenchymal marker genes increased (*CDH2*, *VIM*, and *ZEB1*) indicating EMT was extensive (Fig. 7E–G and I–K, Supplementary Fig. S6).

Discussion

In this report, we studied the behavior of murine lung adenocarcinoma cell lines in a 3D synthetic PEG hydrogel system, specifically focusing on the behavior of a highly plastic, model-metastatic cell line, and the independent influences of matrix mechanics and biochemistry on its epithelial morphogenesis. Our system is a significant advancement over the naturally derived matrix materials widely used in the field because a synthetic system with independently tunable modular components is the only way to reliably study the effect of these factors on cultured cells. Further, because tumor ECM is so complex and cancer cell behavior so exquisitely sensitive to changes in surrounding matrix environment, a "blank slate" system, completely free of uncontrolled sources of bioactivity, is essential to the goal of parsing out the relative significance of particular ECM cues on metastasis to enable identification of the most effective targets for further study and therapeutic development.

We showed that a PEG-based system, with simple bioactivity incorporated through the use of cell-adhesive PEG-RGDS and enzyme-degradable PEG-PQ backbone, was able to induce MET in 344SQ cells to form lumenized, polarized spheres similar to that observed in Matrigel. This observation was important as it suggests that this distinctive behavior is not dependent on excess bioactivity from residual growth factors or the presence of highly bioactive ECM components such as laminin found in high concentrations in Matrigel, but is simply a result of the innate differentiation capacity of these cells in a 3D environment. This observation also established the PEG system as a reliable platform to study matrix-derived influences on cancer cell behavior, a starting point from which the matrix may be further modified to probe for influences on this morphogenesis or EMT.

Two such modifiable characteristics are matrix mechanics and adhesive ligand concentration, which we showed to be highly tunable in our PEG system. The matrices examined in this study ranged from 21 to 55 kPa, but the PEG system can be tailored for either softer or stiffer matrices by varying the PEG base concentration or using a PEG chain with a different number of monomer repeats and molecular weight (22; 34). While all of the hydrogels tested were stiffer than Matrigel-based matrices, all were capable of supporting 344SQ culture and lumenized structure formation, suggesting that the comparatively softer Matrigel environment is not required for epithelial morphogenesis. Any alteration in cell behavior related to this softer environment may be compensated by the excessive bioactivity of the ligand-rich Matrigel.

Comparing 21 and 42 kPa matrices with fixed adhesive ligand, we found that epithelial structures were more organized in stiffer matrices as reflected by the rate and extent of lumenization and differences in sphere development and polar organization. This result runs counter to much of the work in the field that suggests high matrix stiffness favors less tumor organization and enhanced progression (5–7). The disparity may simply highlight the unpredictability of natural matrix biochemistry. Despite best efforts to incorporate similar bioactivity or mechanics, other investigators have shown that the same cells behave differently when cultured on Matrigel or other materials including collagen (35), naturally derived materials such as small intestinal submucosa (36) and polyacrylamide (37), suggesting it is very difficult to control for bioactivity in natural matrices such as Matrigel.

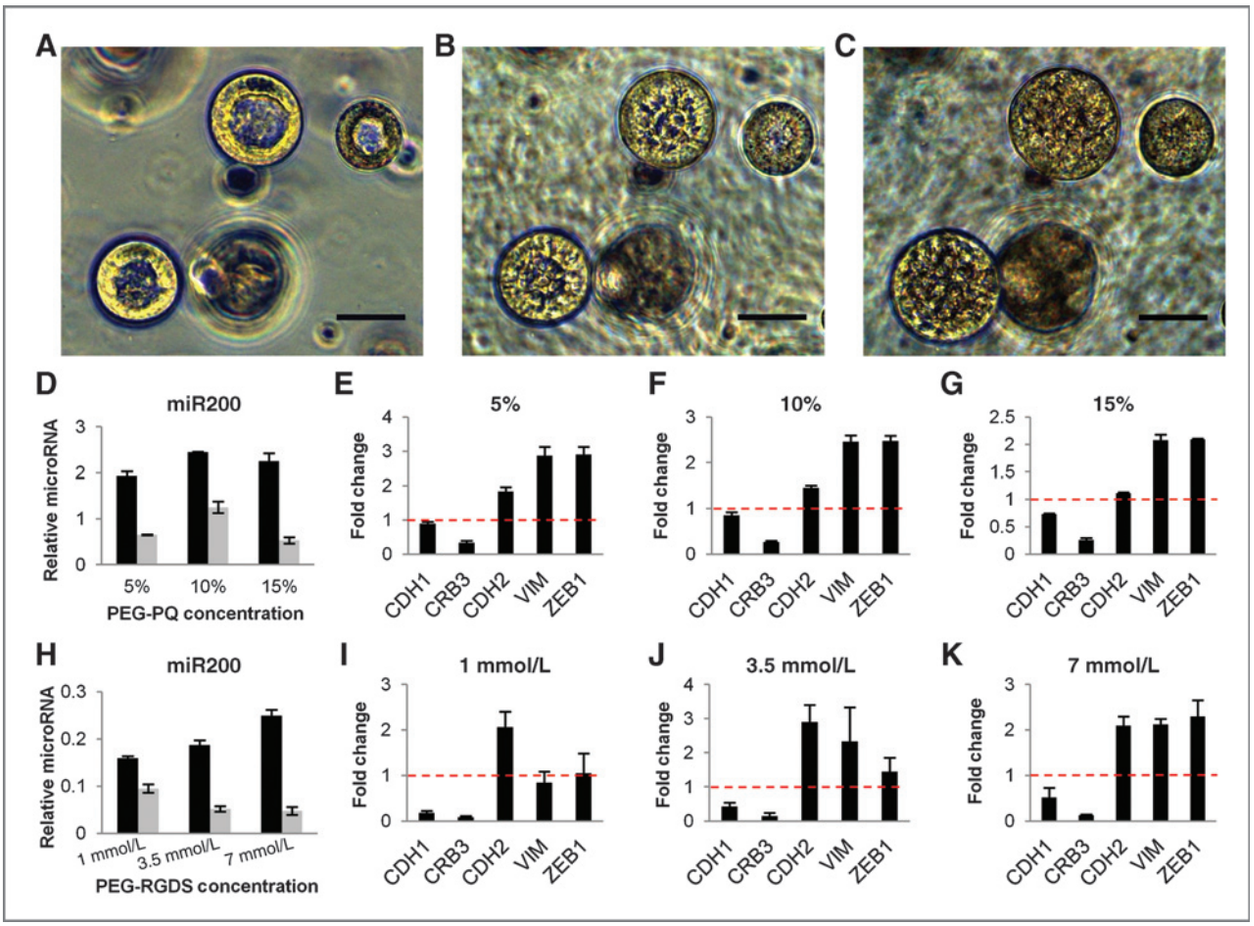

Figure 7. PEG-encapsulated structures show EMT-related morphologic, epigenetic, and gene expression changes with exposure to TGF-β. A–C, bright-field images of lumenized spheres encapsulated in a 5% PEG-PQ, 7 mmol/L PEG-RGDS hydrogel at 12 days in culture before 5 ng/mL TGF-β exposure (A) show breakdown of lumen organization after 1 day of treatment (B) and complete lumen filling and loss of organization after 4 days (C). Scale bar, 50 μm. D–K, q-PCR data for miR-200b before (black bars) and after (gray bars) TGF-β and fold change in mRNA of EMT-related genes with TGF-β treatment in matrices with 3.5 mmol/L PEG-RGDS and varied stiffness (D–G) and matrices with fixed 5% PEG-PQ stiffness and varied PEG-RGDS concentration (H–K) show a decrease in miR-200, decreased expression of epithelial genes (*CDH1* and *CRB3*), and increased expression of mesenchymal genes (*CHD2*, *VIM*, and *ZEB1*) in all matrix formulations following exposure consistent with EMT-related genetic and epigenetic changes seen in 344SQ in Matrigel cultures (for every formulation, miR-200b before vs. after TGF-β, $P < 0.01$). miR-200 is expressed relative to miR16 levels and fold change mRNA relative to *L32* mRNA levels.

Our work was also an effort to disentangle mechanics from bioactivity, a difficult task with natural matrices in which mechanics and ligand density often change concordantly. Discerning the independent contribution of these factors is important given that collagen density, organization, and cross-linking are thought to promote tumor progression (3–5). Indeed, when investigators have deployed synthetic systems with better control over biochemistry and biomechanics, first using 2D polyacrylamide gels, in some cases cancer cells actually adopt a more benign, differentiated state on the stiffer substrate tested or display peak tumorogenic activity in matrices of intermediate stiffness (38–40). A few reports have transitioned this effort into 3D, finding a diminished invasive phenotype in the stiffer formulation of a hyaluronic acid based gel and enhanced epithelialization in stiffer collagen gels cross-linked with bioinert PEG (21; 41). However, the 2D polyacrylamide studies may offer limited insight into the more physiologic behaviors seen in 3D environments. The 3D systems are also imperfect as, despite attempts to control ligand concentration (21) and use bioinert cross-linkers (41), both of the bulk matrix components used are still themselves bioactive, inevitably leading to biochemical changes with increased cross-linking and stiffening.

In addition, while the bulk of work in the field has been done using a collection of the same commonly studied breast cancer model lines, when other cell lines have been examined, the matrix stiffness-related behavior observed is often highly dependent on the identity of the cell line tested or the nature and extent of its malignant transformation (8; 38; 39; 42–44). The cell lines studied here may exhibit either a different response to matrix stiffness or a higher degree of rigidity independence than the commonly used breast lines (8). Further, because very little work in the field has been done using cell lines that specifically and reliably model human

lung adenocarcinoma, our work may highlight unique influences of matrix stiffness on metastatic properties of lung adenocarcinoma.

We also observed a pro-organizational effect of adhesive ligand in experiments altering PEG-RGDS concentration at a fixed matrix stiffness. This result is interesting in the context of results from the bulk of the field showing that a higher ligand concentration, usually collagen, leads to more aggressive tumors (3; 5). This disparity suggests that the identity of ECM ligand and the integrins subsequently bound are crucial to understanding the effect of ECM biochemistry on tumor progression. While little work in this regard has been done with fibronectin, from which RGDS is derived, this point is driven home by the many studies showing that, in contrast to collagen, increased laminin concentration promotes epithelial morphogenesis (35; 37). The PEG system has a unique advantage in that specific peptide sequences or domains from these large ECM molecules may be incorporated with high control and examined for a specific effect whereas, in other matrices, incorporation of a whole molecule with its multiple integrin binding sites may make the system too convoluted, leaving some matrix-derived signaling and gene expression events intractable.

Finally, we observed a repression of miR-200 levels following TGF-β exposure and concomitant shift in EMT marker gene expression. First, this finding is significant as it shows an ability to harvest and collect RNA from a 3D synthetic system, a nontrivial challenge to overcome when transitioning from natural to synthetic matrices. Furthermore, these epigenetic and gene expression changes show that the PEG-encapsulated cells engage physiological regulators of EMT, and that PEG is a useful 3D platform with which to study transcriptional events in response to extracellular signals. Moving forward, because the unmodified PEG matrix is a completely bioinert material, this system will enable much more robust study of additional ECM ligands and biochemical cues that may promote EMT and metastasis. In this vein, future work may modify the PEG system with additional peptides to engage different integrins or incorporate covalently tethered matrix-derived or cell–cell contact proteins that are integral to EMT. In addition, future studies may seek to use patterning techniques already deployed in tissue engineering applications to study 3D spatial relationships between tumors and ECM influences in an entirely new area of investigation (29; 45).

Disclosure of Potential Conflicts of Interest

No potential conflicts of interest were disclosed.

Authors' Contributions

Conception and design: B.J. Gill, D.L. Gibbons, J.E. Saik, Z.H. Rizvi, J.L. West
Development of methodology: B.J. Gill, D.L. Gibbons, J.E. Saik, Z.H. Rizvi, J.L. West
Acquisition of data (provided animals, acquired and managed patients, provided facilities, etc.): B.J. Gill, D.L. Gibbons, L.C. Roudsari, J.E. Saik, Z.H. Rizvi, J.D. Roybal, J.M. Kurie
Analysis and interpretation of data (e.g., statistical analysis, biostatistics, computational analysis): B.J. Gill, D.L. Gibbons, J.E. Saik, Z.H. Rizvi, J.D. Roybal, J.M. Kurie, J.L. West
Writing, review, and/or revision of the manuscript: B.J. Gill, D.L. Gibbons, J. L. West
Administrative, technical, or material support (i.e., reporting or organizing data, constructing databases): B.J. Gill, J.D. Roybal
Study supervision: D.L. Gibbons, J.L. West

Acknowledgments

The authors would like to thank the members of the West, Kurie, and Gibbons laboratories for assistance and comments on the work.

Grant Support

NIH R01 CA157450 (J.M. Kurie and J.L. West). NIH Biotechnology Training Program, 5T32 GM008362-19 (B.J. Gill). J.M. Kurie is the Elza and Ina A. Shackelford Endowed Professor in Lung Cancer Research. D.L. Gibbons was supported by NCI K08 CA151651, an International Association for the Study of Lung Cancer Fellow Grant, and received financial support from the Division of Cancer Medicine Advanced Scholars Program (MD Anderson Cancer Center). J. D. Roybal was supported by a career development award from the UT Southwestern/MD Anderson Cancer Center Lung Specialized Program of Research Excellence (P50 CA70907). Z.H. Rizvi was supported by the HHMI-Medical Research Fellows Program.

The costs of publication of this article were defrayed in part by the payment of page charges. This article must therefore be hereby marked *advertisement* in accordance with 18 U.S.C. Section 1734 solely to indicate this fact.

Received March 7, 2012; revised July 25, 2012; accepted August 13, 2012; published OnlineFirst September 4, 2012.

References

1. Thiery JP, Acloque H, Huang RYJ, Nieto MA. Epithelial-mesenchymal transitions in development and disease. Cell 2009;139:871–90.
2. Provenzano PP, Inman DR, Eliceiri KW, Trier SM, Keely PJ. Contact guidance mediated three-dimensional cell migration is regulated by Rho/ROCK-dependent matrix reorganization. Biophys J 2008;95:5374–84.
3. Provenzano PP, Inman DR, Eliceiri KW, Knittel JG, Yan L, Rueden CT, et al. Collagen density promotes mammary tumor initiation and progression. BMC Med 2008;6:11.
4. Provenzano PP, Eliceiri KW, Campbell JM, Inman DR, White JG, Keely PJ. Collagen reorganization at the tumor-stromal interface facilitates local invasion. BMC Med 2006;4:38.
5. Levental KR, Yu H, Kass L, Lakins JN, Egeblad M, Erler JT, et al. Matrix crosslinking forces tumor progression by enhancing integrin signaling. Cell 2009;139:891–906.
6. Paszek MJ, Zahir N, Johnson KR, Lakins JN, Rozenberg GI, Gefen A, et al. Tensional homeostasis and the malignant phenotype. Cancer Cell 2005;8:241–54.
7. Provenzano PP, Inman DR, Eliceiri KW, Keely PJ. Matrix density-induced mechanoregulation of breast cell phenotype, signaling and gene expression through a FAK-ERK linkage. Oncogene 2009;28:4326–43.
8. Tilghman RW, Cowan CR, Mih JD, Koryakina Y, Gioeli D, Slack-Davis JK, et al. Matrix rigidity regulates cancer cell growth and cellular phenotype. PloS One 2010;5:e12905.
9. Ulrich TA, de Juan Pardo EM, Kumar S. The mechanical rigidity of the extracellular matrix regulates the structure, motility, and proliferation of glioma cells. Cancer Res 2009;69:4167–74.
10. Alexander NR, Branch KM, Parekh A, Clark ES, Iwueke IC, Guelcher SA, et al. Extracellular matrix rigidity promotes invadopodia activity. Curr Biol 2008;18:1295–9.
11. Zheng S, El-Naggar AK, Kim ES, Kurie JM, Lozano G. A genetic mouse model for metastatic lung cancer with gender differences in survival. Oncogene 2007;26:6896–904.
12. Gibbons DL, Lin W, Creighton CJ, Zheng S, Berel D, Yang Y, et al. Expression signatures of metastatic capacity in a genetic mouse model of lung adenocarcinoma. PloS One 2009;4:e5401.

13. Gibbons DL, Lin W, Creighton CJ, Rizvi ZH, Gregory PA, Goodall GJ, et al. Contextual extracellular cues promote tumor cell EMT and metastasis by regulating miR-200 family expression. Genes Dev 2009;23:2140–51.
14. Schliekelman MJ, Gibbons DL, Faca VM, Creighton CJ, Rizvi ZH, Zhang Q, et al. Targets of the tumor suppressor miR-200 in regulation of the epithelial-mesenchymal transition in cancer. Cancer Res 2011;71:7670–82.
15. Yang Y, Ahn YH, Gibbons DL, Zang Y, Lin W, Thilaganathan N, et al. The Notch ligand Jagged2 promotes lung adenocarcinoma metastasis through a miR-200–dependent pathway in mice. J Clin Invest 2011;121:1373–85.
16. Hughes CS, Postovit LM, Lajoie GA. Matrigel: a complex protein mixture required for optimal growth of cell culture. Proteomics 2010;10:1886–90.
17. Vukicevic S, Kleinman HK, Luyten FP, Roberts AB, Roche NS, Reddi A. Identification of multiple active growth factors in basement membrane Matrigel suggests caution in interpretation of cellular activity related to extracellular matrix components. Exp Cell Res 1992;202:1–8.
18. Lutolf MP, Hubbell JA. Synthetic biomaterials as instructive extracellular microenvironments for morphogenesis in tissue engineering. Nat Biotechnol 2005;23:47–55.
19. Gribova V, Crouzier T, Picart C. A material's point of view on recent developments of polymeric biomaterials: control of mechanical and biochemical properties. J Mater Chem 2011;21:14354–66.
20. Nemir S, West JL. Synthetic materials in the study of cell response to substrate rigidity. Ann Biomed Eng 2010;38:2–20.
21. Ananthanarayanan B, Kim Y, Kumar S. Elucidating the mechanobiology of malignant brain tumors using a brain matrix-mimetic hyaluronic acid hydrogel platform. Biomaterials 2011;32:7913–23.
22. Nemir S, Hayenga HN, West JL. PEGDA hydrogels with patterned elasticity: novel tools for the study of cell response to substrate rigidity. Biotechnol Bioeng 2010;105:636–44.
23. Miroshnikova Y, Jorgens D, Spirio L, Auer M, Sarang-Sieminski A, Weaver V. Engineering strategies to recapitulate epithelial morphogenesis within synthetic three-dimensional extracellular matrix with tunable mechanical properties. Phys Biol 2011;8:026013.
24. Xi T, Fan C, Feng X, Wan Z, Wang C, Chou L. Cytotoxicity and altered c-myc gene expression by medical polyacrylamide hydrogel. J Biomed Mater Res A 2006;78:283–90.
25. Franco CL, Price J, West JL. Development and optimization of a dual-photoinitiator, emulsion-based technique for rapid generation of cell-laden hydrogel microspheres. Acta Biomater 2011;7:3267–76.
26. Moon JJ, Saik JE, Poché RA, Leslie-Barbick JE, Lee S-H, Smith AA, et al. Biomimetic hydrogels with pro-angiogenic properties. Biomaterials 2010;31:3840–7.
27. Saik JE, Gould DJ, Keswani AH, Dickinson ME, West JL. Biomimetic hydrogels with immobilized ephrinA1 for therapeutic angiogenesis. Biomacromolecules 2011;12:2715–22.
28. Lazard ZW, Heggeness MH, Hipp JA, Sonnet C, Fuentes AS, Nistal RP, et al. Cell-based gene therapy for repair of critical size defects in the rat fibula. J Cell Biochem 2011;112:1563–71.
29. Hoffmann JC, West JL. Three-dimensional photolithographic patterning of multiple bioactive ligands in poly(ethylene glycol) hydrogels. Soft Matter 2010;6:5056–63.
30. Lutolf M, Lauer-Fields J, Schmoekel H, Metters A, Weber F, Fields G, et al. Synthetic matrix metalloproteinase-sensitive hydrogels for the conduction of tissue regeneration: engineering cell-invasion characteristics. Proc Natl Acad Sci U S A 2003;100:5413–8.
31. West JL, Hubbell JA. Polymeric biomaterials with degradation sites for proteases involved in cell migration. Macromolecules 1999;32:241–44.
32. Cruise GM, Scharp DS, Hubbell JA. Characterization of permeability and network structure of interfacially photopolymerized poly(ethylene glycol) diacrylate hydrogels. Biomaterials 1998;19:1287–94.
33. Browning MB, Wilems T, Hahn M, Cosgriff-Hernandez E. Compositional control of poly(ethylene glycol) hydrogel modulus independent of mesh size. J Biomed Mater Res A 2011;98A:268–73.
34. Hahn M, McHale M, Wang E, Schmedlen R, West J. Physiologic pulsatile flow bioreactor conditioning of poly(ethylene glycol)-based tissue engineered vascular grafts. Ann Biomed Eng 2007;35:190–200.
35. Stadler E, Dziadek M. Extracellular matrix penetration by epithelial cells is influenced by quantitative changes in basement membrane components and growth factors. Exp Cell Res 1996;229:360–9.
36. Hurst RE, Kyker KD, Bonner RB, Bowditch RD, Hemstreet GP III. Matrix-dependent plasticity of the malignant phenotype of bladder cancer cells. Anticancer Res 2003;23:3119–28.
37. Alcaraz J, Xu R, Mori H, Nelson CM, Mroue R, Spencer VA, et al. Laminin and biomimetic extracellular elasticity enhance functional differentiation in mammary epithelia. EMBO J 2008;27:2829–38.
38. Lam WA, Cao L, Umesh V, Keung AJ, Sen S, Kumar S. Extracellular matrix rigidity modulates neuroblastoma cell differentiation and N-myc expression. Mol Cancer 2010;9:35.
39. Kostic A, Lynch CD, Sheetz MP. Differential matrix rigidity response in breast cancer cell lines correlates with the tissue tropism. PloS One 2009;4:e6361.
40. Parekh A, Ruppender NS, Branch KM, Sewell-Loftin MK, Lin J, Boyer PD, et al. Sensing and modulation of invadopodia across a wide range of rigidities. Biophys J 2011;100:573–82.
41. Liang Y, Jeong J, Devolder RJ, Cha C, Wang F, Tong YW, et al. A cell-instructive hydrogel to regulate malignancy of 3D tumor spheroids with matrix rigidity. Biomaterials 2011;32:9308–15.
42. Tseng Q, Wang I, Duchemin-Pelletier E, Azioune A, Carpi N, Gao J, et al. A new micropatterning method of soft substrates reveals that different tumorigenic signals can promote or reduce cell contraction levels. Lab Chip 2011;11:2231–40.
43. Indra I, Beningo KA. An *in vitro* correlation of metastatic capacity, substrate rigidity and ECM composition. J Cell Biochem 2011;112:3151–8.
44. Baker EL, Srivastava J, Yu D, Bonnecaze RT, Zaman MH. Cancer cell migration: integrated roles of matrix mechanics and transforming potential. PLoS One 2011;6:e20355.
45. Lee SH, Moon JJ, West JL. Three-dimensional micropatterning of bioactive hydrogels via two-photon laser scanning photolithography for guided 3D cell migration. Biomaterials 2008;29:2962–8.